Journal of Power Sources 195 (2010) 2283–2290

Contents lists available at ScienceDirect

Journal of Power Sources

journal homepage: www.elsevier.com/locate/jpowsour

Improved modelling of the fuel cell power module within a system-level model for solid-oxide fuel cell cogeneration systems

Michael Carl[a,*], Ned Djilali[a], Ian Beausoleil-Morrison[b]

[a] Institute for Integrated Energy Systems and Department of Mechanical Engineering, University of Victoria, Victoria, Canada
[b] Mechanical and Aerospace Engineering, Carleton University, Ottawa, Canada

ARTICLE INFO

Article history:
Received 16 September 2009
Received in revised form 15 October 2009
Accepted 16 October 2009
Available online 29 October 2009

Keywords:
Solid-oxide fuel cell
Fuel cell
Cogeneration
ESP-r
System-level model

ABSTRACT

A generic system-level model for SOFC cogeneration devices has been developed under the umbrella of an International Energy Agency/Energy Conservation in Buildings and Community Systems project known as Annex 42. This paper addresses a limitation of the Annex 42 model by developing a more refined semi-mechanistic treatment for the fuel cell power module (FCPM). The electrochemical, thermal, and reformation modelling methods as well as techniques for treating the FCPM's balance of plant are first described. The methods used to calibrate and validate the enhanced model using previously collected data from a 2.8 kW_{AC} prototype SOFC cogeneration device are then discussed. Excellent agreement was found between model predictions and the measurements. The new modelling capabilities are then demonstrated through a parametric study that examines the influences of fuel utilization, excess air ratio and stack temperature.

1. Introduction

Solid-oxide fuel cells (SOFC) are currently the subject of much interest from the research community. This is because: (1) SOFCs have a high electrical energy conversion efficiency compared to other similar technologies [1]; (2) SOFCs operate at 800–1000 °C generating quality thermal energy, which can be used for further electrical conversion or heating; (3) SOFCs can use a number of different fuels including hydrogen, methane, carbon monoxide and other hydrocarbons; (4) SOFCs offer reduced emissions over other technologies because of their increased efficiency, and depending on the type of fuel, lack of combustion by-products.

Researchers have focused on numerous applications for SOFC's including; small scale electricity generating plants (<100 kW), bottoming cycle electricity generating plants, and combined heat and power production (or cogeneration) [2–6]. Each of these topics is a worthwhile area of research; however, cogeneration is of particular interest because it can offer the highest overall energy efficiency. This is accomplished through the high electrical conversion efficiency of the SOFC unit itself combined with the use of the thermal energy given off by the unit for heating. As a result, cogeneration offers an intriguing alternative to current power and heat generation technologies.

SOFC cogeneration is possible at a number of scales, from single family residential (1–5 kW) to small central power plants (100 kW to 1 MW). Residential systems offer more immediate promise because they can easily be incorporated into existing heating systems. On the other hand the power plant scale build would require the installation of a district heating system, which is both costly and difficult to do in a retrofit scenario. Residential systems also offer the advantages of distributed power. According to the Ontario Power Authority (OPA) distributed power can help to reduce peak demands as well as reduce transmission and distribution congestion [7]. Therefore, residential cogeneration has a distinct advantage over the plant scale for becoming a viable electricity and thermal production technology.

The present study was conducted under the umbrella of Annex 42 of the International Energy Agency Energy Conservation in Buildings and Community Systems programme (IEA/ECBCS) [8,9]. Annex 42 is an international research project focusing on the development and validation of models of fuel cell and other cogeneration technologies in the building environment, and the integration of these models into existing, open source whole-building simulation programs. In this work we present a generic model for SOFC residential cogeneration systems and its implementation into the building simulation analysis tool ESP-r [10]. ESP-r is an open source building simulation tool whose modelling methodologies are described in detail by Clarke [11]. This modelling approach allows the concurrent simulation of SOFC cogeneration devices and building thermal and electrical demands, all subject to climatological and occupant behaviour influences.

* Corresponding author. Tel.: +1 289 839 0588; fax: +1 519 823 1316.
E-mail address: michael.j.carl@gmail.com (M. Carl).

0378-7753/$ – see front matter © 2009 Elsevier B.V. All rights reserved.
doi:10.1016/j.jpowsour.2009.10.052

Beausoleil-Morrison and Lombardi [11] have demonstrated how the Annex 42 model can be calibrated (tuned) to represent the electrical and thermal performance of a 2.8 kW_{AC} prototype SOFC cogeneration device and Beausoleil-Morrison (submitted article) has demonstrated the model's validity through comparison of model predictions with measurements.

The Annex 42 model has contributed towards the accurate assessment of the performance of SOFC cogeneration. However, the model's applicability is limited by requiring measured data to calibrate a device's electrical conversion efficiency. The current work sets out to address this limitation by proposing a more refined treatment of the fuel cell power module (FCPM) within the Annex 42 model.

The next section outlines the proposed enhancements to the Annex 42 model. The calibration and validation of this new modelling method is treated in the following section. The new capabilities enabled by these enhancements are then demonstrated through a parametric study.

2. Modelling approach

The control volume defining the FCPM contains the fuel cell stack, the stack burner, the after burner, the fuel and air preheaters, the fuel desulfurizer, and the air filter. The boundary of this control volume is represented by the heavy dashed line in Fig. 1. The key FCPM variables are fuel flow rates to the stack and stack burner, inlet/exhaust gas composition and temperature, and electrical conversion efficiency. Based on these required outputs a zero dimensional energy balance and electrochemical model has been developed. The model considers fuel reformation, balance of plant (BOP) power requirements, cell polarization, and an energy balance of the fuel cell stack (FCS). The control volume representing the FCS which is used for the cell polarization calculations and energy balance as described below is also shown in Fig. 1. The data gathered by Beausoleil-Morrison and Lombardi [11] from a prototype SOFC cogeneration unit are used to calibrate this model for this particular device. As such, the new model can represent that particular SOFC system as well as, with slight modifications, other designs or hypothetical SOFC cogeneration system.

The electrical efficiency of the FCPM is defined as:

$$\eta_{\mathrm{FCPM}} = \frac{P_{\mathrm{stack}}}{(\dot{N}_{\mathrm{fuel\text{-}stack}} + \dot{N}_{\mathrm{fuel\text{-}burn}})LHV_{\mathrm{fuel}}} \tag{1}$$

where $\dot{N}_{\mathrm{fuel\text{-}stack}}$ and $\dot{N}_{\mathrm{fuel\text{-}burn}}$ are the fuel requirements (kmol s^{-1}) of the fuel cell stack (FCS) and the stack burner, respectively. The stack burner is used to maintain the temperature within the stack. The stack burner is only activated when the temperature in the FCS drops bellow the desired threshold. When the stack burner is activated the fuel flow rate is constant. The stack temperature is determined by the FCS control volume energy balance. The FCS fuel flow rate is determined based on the FCS efficiency:

$$\dot{N}_{\mathrm{fuel\text{-}stack}} = \frac{P_{\mathrm{stack}}}{\eta_{\mathrm{FCS}} LHV_{\mathrm{fuel}}} \tag{2}$$

where η_{FCS} is the efficiency of the fuel cell stack and P_{stack} is the output power (W) of the stack. The stack power is defined as:

$$P_{\mathrm{stack}} = P_{\mathrm{el}} + P_{\mathrm{dc,ann}} \tag{3}$$

where P_{el} represents the power required by the power conditioning unit (PCU) and $P_{\mathrm{dc,ann}}$ represents the parasitic power (W) draw of the BOP.

2.1. BOP power requirements

The BOP components support the operation of the FCPM, but have a DC power draw associated with them. In the case of the design of this prototype there is also a substantial voltage loss between the stack and the power conditioning unit (PCU). The BOP power draw and the voltage drop are represented with the following equation:

$$P_{\mathrm{dc,ann}} = P_{\mathrm{dc,comp}} + P_{\mathrm{IV}} = \varepsilon_{\mathrm{ann\text{-}0}} \exp(\varepsilon_{\mathrm{ann\text{-}1}} P_{\mathrm{el}}) + \varepsilon_{\mathrm{IV\text{-}0}} \exp(\varepsilon_{\mathrm{IV\text{-}1}} P_{\mathrm{el}}) \tag{4}$$

where $P_{\mathrm{dc,comp}}$ is the power (W) draw of the BOP components and P_{IV} is the power (W) loss due to the ohmic losses in the cabling between the stack and the PCU. The ε terms represent the empirical constants. The form of Eq. (4) was chosen because exact information regarding the BOP components was not known. However Eq. (4) can be generalized in order to test hypothetical systems:

$$P_{\mathrm{dc,ann}} = \sum_i P_i(n_1, n_2 \ldots) \tag{5}$$

where i represents the hypothetical BOP component, and n represents the variable of which i is a function. For example, power to the air supply blower would be a function of the pressure change and air flow rate.

2.2. Methane reformation

SOFCs are typically fuelled with either hydrogen or methane. If methane is used then reformation must be considered. The chemical equations representing methane reformation are as follows:

$$CH_4 + H_2O \rightarrow CO + 3H_2 \tag{6}$$

$$CO + H_2O \rightarrow CO_2 + H_2 \tag{7}$$

$$H_2 + \tfrac{1}{2}O_2 \rightarrow H_2O \tag{8}$$

where Eq. (6) is the reformation reaction, Eq. (7) is the gas-shift reaction and Eq. (8) is the electrochemical conversion reaction of hydrogen. In the current study Eq. (6) is considered to be completely reformed. This can be justified by the works of [12], who found that methane completely reforms (less then 1% persisting) within the SOFC. Eq. (7) can be characterized using equilibrium because its reaction is fast and weakly exothermic [13]:

$$K_{\mathrm{s}} = \frac{p_{H_2} p_{CO_2}}{p_{CO} p_{H_2O}} \tag{9}$$

where p_{i} is the partial pressure of the respective gas and K is the equilibrium constant. The K values for both the reformation and shifting reaction have been determined by Bossel et al. [14] as a function of temperature:

$$\log\ K_{\mathrm{s}} = AT^4 + BT^3 + CT^2 + DT + E \tag{10}$$

where T is the temperature of the reaction and A–E are empirical constants.

Given known inlet molar flow rates for the gases and known fuel utilization for the system, Chan et al. [2] have determined a method for solving Eq. (9). They used x, y, and z to represent the molar flows of methane, carbon monoxide and hydrogen in the reactions. Re-writing Eq. (9) in terms of molar flow rates and the electrochemical reaction for determination of the hydrogen flow, the following equations are developed:

$$K_{\mathrm{s}} = \frac{(CO_2^I + y)(H_2^I + 3CH_4^I + y - z)}{(CO^I + CH_4^I - y)(H_2O^I - x - y + z)} \tag{11}$$

$$z = U_{\mathrm{f}}(H_2^I + 3x + y) \tag{12}$$

where the chemical symbols represent the initial (or inlet) molar flow rates and x, y, z represent the molar flow rates of methane, carbon monoxide and hydrogen, respectively. Since x is the molar flow of CH_4 and that reaction has been assumed to be complete x can

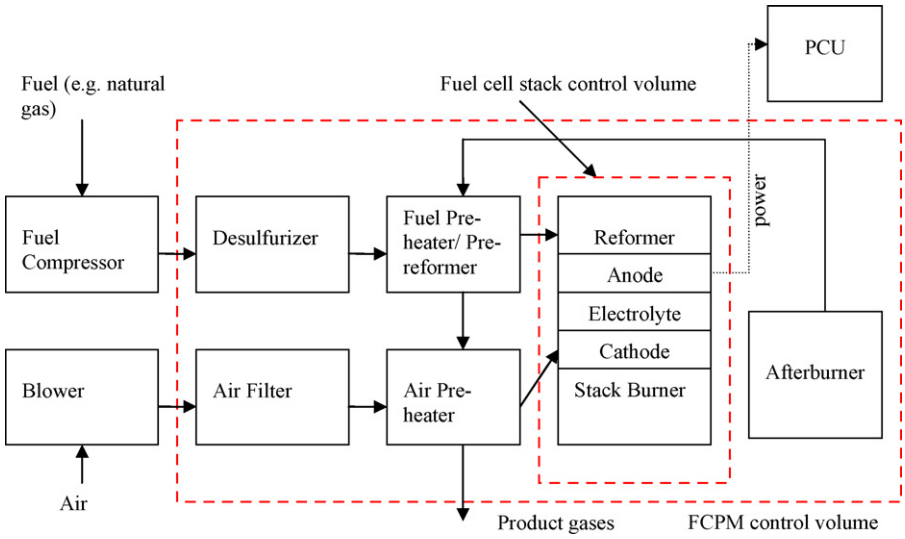

Fig. 1. Schematic giving generic configuration for the FCPM.

be replaced with the inlet CH_4 flow rate. Eq. (12) can then be solved to give the mole fraction of each of the constituents. Lisbona et al. [5] found that the remaining CO from the gas-shift reaction does not produce electricity in the SOFC and is subsequently neglected.

2.3. Electrochemical model

The power which must be generated by the stack is related to the stack current and voltage such that:

$$P_{\text{stack}} = n_{\text{cells-parrallel}} I_{\text{cell}} n_{\text{cells-series}} V_{\text{cell}} \tag{13}$$

where $n_{\text{cells-parallel}}$ and $n_{\text{cells-series}}$ are the number of cells in parallel and series in the fuel cells stack arrangement, respectively, and I_{cell} and V_{cell} are the current (A) and voltage (V) of a single cell. V_{cell} can be expressed as the Nernst voltage minus losses due to current-flow. Within the model, activation polarization, ohmic losses and concentration polarization are considered, such that:

$$V_{\text{cell}} = E_{\text{r}} - V_{\text{act}} - V_{\text{ohm}} - V_{\text{con}} \tag{14}$$

where E_{r} is the Nernst reversible voltage (V), V_{act} is the activation polarization, V_{ohm} is the ohmic loss, and V_{con} is the concentration polarization (V) of each cell. The model assumes that all reactant gases behave ideally, and that the operating pressure is 1 bar.

2.3.1. Activation polarization

The electrochemical reaction in the fuel cell requires energy to proceed. The voltage loss associated with this process is characterized by the Butler–Volmer equation:

$$i = i_{\text{o}} \left[\exp\left(\frac{\beta n_{\text{e}} F V_{\text{act}}}{RT} \right) - \exp\left(\frac{-(1-\beta) n_{\text{e}} F V_{\text{act}}}{RT} \right) \right] \tag{15}$$

where i_{o} is the exchange current density, β is the transfer coefficient, T is the temperature and R is the universal gas constant. If $\beta = 0.5$ is assumed, the Butler–Volmer equation can be solved explicitly such that [15]:

$$V_{\text{act}}^{\text{an}} = \frac{2RT}{n_{\text{e}}F} \sinh^{-1}\left(\frac{i}{2i_{\text{o,an}}} \right) \tag{16}$$

$$V_{\text{act}}^{\text{ca}} = \frac{2RT}{n_{\text{e}}F} \sinh^{-1}\left(\frac{i}{2i_{\text{o,ca}}} \right)$$

where the super/subscripts an and ca stand for the cathode and anode side reactions, respectively. The exchange current density (i_{o}) (A cm^{-2}) is then the only parameter remaining to be determined. The exchange current density can be expressed by [3,15–17]:

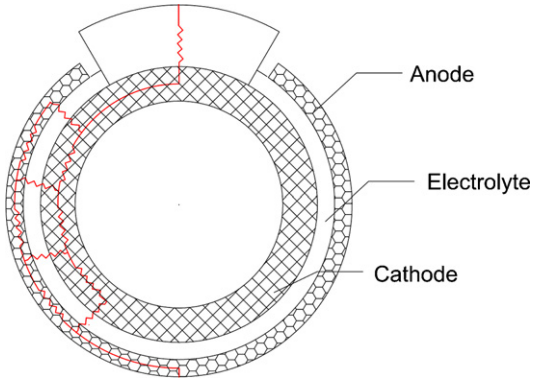

Fig. 2. Equivalent resistance circuit for a single SOFC tube.

$$i_{\text{o,an}} = \gamma_{\text{an}} p_{\text{H}_2} p_{\text{H}_2\text{O}}^{m} \exp\left(-\frac{E_{\text{act,an}}}{RT} \right) \tag{18}$$

$$i_{\text{o,ca}} = \gamma_{\text{ca}} p_{\text{O}_2}^{0.25} \exp\left(-\frac{E_{\text{act,ca}}}{RT} \right) \tag{19}$$

where γ_{an} and γ_{ca} are the pre-exponential coefficients m is an empirical coefficient and E_{act} is the activation energy.

2.3.2. Ohmic losses

Ohmic losses are caused by the resistivity of the SOFC materials to current-flow. To determine the Ohmic losses, an equivalent resistance [15,17–20] is employed coupled with Ohm's law.

$$V_{\text{ohm}} = iR_{\text{eq}} \tag{20}$$

where R_{eq} is the area specific equivalent resistance (ohm cm^2) of the cell.

The equivalent resistance is presented in Fig. 2. Nisancioglu [21] has developed an analytical solution to the equivalent resistant of a tubular SOFC [21]. This solution with corrections for the temperature dependence of conductivity [12] is as follows:

$$R_1 = \frac{[(1/\sigma_{\text{an}}L_{\text{an}})^2 + (1/\sigma_{\text{ca}}L_{\text{ca}})^2]\cosh(Z_{\text{e}}) + (1/\sigma_{\text{an}}L_{\text{an}}\sigma_{\text{ca}}L_{\text{ca}})(2 + Z_{\text{e}}\sinh(Z_{\text{e}}))}{2(\sigma_{\text{el}}/L_{\text{el}})^{1/2}((1/\sigma_{\text{an}}L_{\text{an}}) + (1/\sigma_{\text{ca}}L_{\text{ca}})^{3/2})\sinh(Z_{\text{e}})} \tag{21}$$

$$Z_e = \frac{Path_{el}}{2}\sqrt{\left(\frac{\sigma_{el}}{L_{el}}\right)\left(\frac{1}{\sigma_{an}L_{an}}+\frac{1}{\sigma_{ca}L_{ca}}\right)} \quad (22)$$

$$R_{int} = \frac{L_{int}}{\sigma_{int}A_{int}} \quad (23)$$

$$R_{eq} = \frac{R_1 A_{cell}}{L_{cell}} + R_{int}A_{cell} \quad (24)$$

where the subscripts el and int stand for electrolyte, and interconnect, respectively, L is the layer thickness(cm), σ is the conductivity (Ω^{-1} cm^{-1}) of the material, and A is the area (cm^2) perpendicular to current-flow. L_{cell} refers to the length of the entire cell and $Path_{el}$ is radial distance (circumference) (cm) of the electrolyte.

2.3.3. Concentration polarization

Concentration polarization is the voltage loss due to the limitations of diffusive transport of gases to the reaction sites. The equations that describe the anode and cathode concentration losses are:

$$V_{con}^{an} = \frac{RT}{n_e F}\ln\left(\frac{1-(i/i_{L,H_2})}{1+(i/i_{L,H_2O})}\right) \quad (25)$$

$$V_{con}^{ca} = \frac{RT}{n_e F}\ln\left(1-\frac{i}{i_{L,O_2}}\right) \quad (26)$$

where $i_{L,I}$ is the limiting current density (A cm^{-2}) of the reaction gases. The limiting current density for each species can be determined using the fundamental equation for isothermal transport of gaseous species in porous electrodes [22]. Derivations of these limiting current densities are provided by [20,22]. The equations are as follows:

$$i_{L,H_2} = \frac{n_e F D_{eff,H_2}}{RTL_{an}}p_{H_2} \quad (27a)$$

$$i_{L,H_2O} = \frac{n_e F D_{eff,H_2O}}{RTL_{an}}p_{H_2O} \quad (27b)$$

$$i_{L,O_2} = \frac{n_e F D_{eff,O_2}}{RTL^a(1-p_{O_2}\delta_{O_2})}p_{O_2} \quad (27c)$$

where D_{eff} is the effective diffusion coefficient of each gas, L is the thickness and p is the partial pressure.

In order to evaluate Eqs. (27a)–(27c) the effective diffusion coefficients for each species must be determined in (cm^2 s^{-1}). The effective diffusion coefficient for each species is calculated using binary and Knudsen diffusion coefficients. The methods described by Todd [23] are used for the binary diffusion coefficients and the Knudsen diffusion is expressed through an equation relating the mean-free path to average pore size such that (hydrogen used as example) [20,23]:

$$\frac{1}{D_{eff,H_2}} = \frac{\varepsilon}{\tau}\left(\frac{1}{D_{H_2,k}}+\frac{1}{D_{H_2,H_2O}}\right) \quad (28)$$

$$D_{H_2-H_2O} = \frac{0.00143T^{1.75}}{M_{H_2-H_2O}^{1/2}\left(\nu_{H_2}^{1/3}+\nu_{H_2O}^{1/3}\right)^2 P} \quad (29)$$

$$D_{H_2,k} = 97.0 r_{por}\sqrt{\frac{T}{M_{H_2}}} \quad (30)$$

where ε is porosity, τ is tortuosity, M is molar mass (kg kmol^{-1}), ν is diffusion volume (cm^3) and r_{por} is the pore length (cm). Given a current density, Eqs. (25) and (26) can now be used to determine the concentration polarization losses at the cathode and anode.

2.3.4. Stack resistance

The proposed model thus far has been limited to the cell level polarization and has not considered the coupling of the cells into a stack. There is little research available in the literature dedicated to modelling entire stacks beyond the expedient and simplistic approach of multiplying a cell voltage by the number of cells in the stack [3–5,18,24,19,25–27]. In order to account for the losses observed in excess of the sum of the individual cell losses, the current model proposes an additional voltage loss termed stack resistance voltage. Introducing this additional voltage loss normalized to a single cell, V_{cell} is now:

$$V_{cell} = E_r - V_{act} - V_{ohm} - V_{con} - V_{SR} \quad (31)$$

where V_{SR} is the stack resistance voltage (V) caused by the coupling of the individual cells within the stack. This term was determined from the experimental results used to calibrate the model as described in Section 3.

2.4. Energy balance-fuel cell stack

An energy balance is used in the determination of the FCS temperature. Stack temperature is important as many parameters described in the preceding section are temperature-dependent. Furthermore, if the stack temperature drops bellow a user-specified threshold then the stack burner must be activated. A control volume is drawn around the fuel cell stack and stack burner (FCV) to evaluate the FCS temperature (Fig. 1). The energy equation for this control volume is as follows:

$$(MC_\rho)\frac{\partial T_{FCV}}{\partial t} = \dot{H}_{air} + \dot{H}_{fuel} - \dot{H}_{products} - P_{stack} - q_{skinlosses} \quad (32)$$

where MC_ρ is the thermal capacitance (J K^{-1}) of the FCV and T_{FCV} is the temperature of the fuel cell control volume. $\dot{H}_{air}$, $\dot{H}_{fuel}$ and $\dot{H}_{products}$ are the enthalpy flow rates (J kmol^{-1} s^{-1}) of the air entering, the fuel entering and the product gasses leaving the FCV, respectively. $\dot{H}_{products}$ includes the product H_2O vapour and CO_2 from the electrochemical reaction, the products of the combustion of the un-reacted fuel, and the excess air. Finally, $q_{skinlosses}$ are the heat losses (W) from the fuel cell stack to the surroundings.

The enthalpy of each the constituents is temperature-dependent. Therefore, the temperature of the fuel and air exiting the respective pre-heaters and entering the FCV must be determined. The pre-heaters use the exhaust gases from the fuel cell as hot input streams. However, the exact configuration of these heat exchangers is proprietary knowledge. In the current research, a simple heat exchanger model which can be calibrated using known heat exchanger properties or empirical data is employed. In order to develop this relationship, an idealized heat exchanger representation is used for each of the air and fuel pre-heaters. In this, it is assumed that all the heat extracted from the product gas stream flowing through a heat exchanger is transferred to the air or fuel stream according to:

$$(\dot{N}C_\rho)_{product}(T_{FCV} - T_{products\text{-}FCPM}) = (\dot{N}C_\rho)_i(T_{i,\text{in FCV}} - T_{i,\text{in FCPM}}) \quad (33)$$

where $\dot{N}$ is the molar flow rate (kmol s^{-1}) and C_p is molar heat capacity (J K^{-1} mol^{-1}). The T_i terms represent temperature where the subscript definitions are as follows: stack signifies the fuel cell stack, products-FCPM signifies the gases exiting the FCPM, and i, inFCV refer to either the fuel or air stream entering the fuel cell control volume. The details regarding the calculation of fuel, air, and product gas temperatures entering and exiting the FCPM are described in detail in [9]. The ratio of $\dot{N}\,C_p$ for the products and the reactant (fuel or air) is used as the "heat exchanger effectiveness"

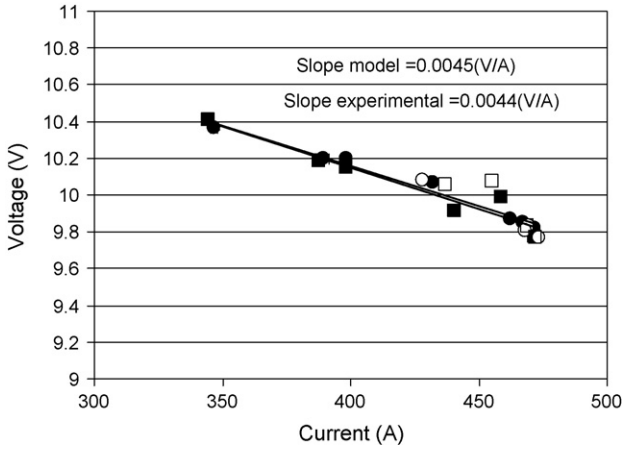

Fig. 3. Comparison of model and experimental results for voltage vs. current performance of the SOFC stack; experimental data used to calibrate model (●), model predictions corresponding to calibration experiment (■), experimental data used to validate model (○), model predictions corresponding to validation experiments (□).

(β_i). The heat exchanger effectiveness can then be used to determine the temperature of the air or fuel entering the FCV:

$$T_{i,\text{in FCV}} = \beta_i(T_{\text{FCV}} - T_{\text{products-FCPM}}) + T_{i,\text{inFCPM}} \quad (34)$$

Finally, if assumptions of an isothermal stack temperature, complete combustions of all gases, and that the gases reach the stack temperature before exiting the stack, are made, then $T_{\text{stack}} = T_{\text{products}} = T_{\text{FCV}} = T$ (electrochemical reactions). The molar enthalpy of the products can now be evaluated at T_{stack}. If the stack temperature drops below a certain threshold then the stack burner is turned on. The energy balance must in turn be modified to account for this additional energy flow:

$$(MC_p)\frac{\partial T_{\text{FCS}}}{\partial t} = \dot{H}_{\text{air}} + \dot{H}_{\text{fuel}} + \dot{H}_{\text{stack-burn}} - \dot{H}_{\text{products}} - P_{\text{stack}} - q_{\text{skinlosses}} \quad (35)$$

where $\dot{H}_{\text{stack-burrn}}$ is the enthalpy flow of the stack burner.

3. Calibration and validation

The model described in the previous section was incorporated into the Annex 42 model in the ESP-r program. This new model was then calibrated and validated using data from the 2.8 kW_{AC} prototype device examined by Beausoleil-Morrison and Lombardi [11]. The data used to calibrate the model was taken from a series of experiments conducted on the 2.8 kW_{AC} prototype device under varied and controlled boundary conditions [28]. Additional data taken from a distinct set of experiments with *different* boundary conditions then those used for calibration were used for the validation data. Fig. 3 presents the stack voltage versus stack current for the model and experimental results. The figure contains two comparative sets: calibration and validation. The calibration data were used to tune the model, specifically the heat exchanger and P_{el} portions, to correspond with the experimental results. Validation data was used for "blind" comparison between the model and the experimental results, as discussed above. The experimental results are presented as averages of long run times on the order of hours. Similarly the results from the Annex 42 model with the new capabilities are generated from long simulation times, in which the P_{el}'s used in the experiments, were used as inputs into the model. The U_f in the stack, the excess air ratio and the average stack temperature were also consistent between the series of model simulations and the experimental data they were being compared to. However, it should be noted that those parameters were not held constant in each separate experiment or simulation run. The average operating conditions for experimental data are presented in Table 1.

Table 1
Calibration and validation operation parameters (lambda represents excess air ratio) measured during each of the experimental runs using the prototype system. The parameters are averages of the values collected over the course of the experiments which ranged in length from 1 to 10 h.

Case	P_{el} (W)	Lambda	Fuel utilization	Temperature (K)
Calibration 1	3010	2.59	0.756	1245
Calibration 2	3283	2.68	0.756	1255
Calibration 3	3353	2.64	0.733	1257
Calibration 4	3580	2.58	0.733	1262
Calibration 5	3728	2.67	0.730	1262
Calibration 6	3712	2.63	0.731	1263
Calibration 7	3728	2.60	0.731	1262
Validation 1	3600	2.54	0.729	1258
Validation 2	3746	2.68	0.730	1262
Validation 3	3743	2.64	0.732	1262
Validation 4	3715	2.55	0.730	1250

Fig. 3 demonstrates good agreement between the model and experimental results; the slopes of the lines are 0.0045 and −0.0044 ($V A^{-1}$), respectively. Also, the average relative and root mean square errors were less then 1% for the current and voltage. Both the model and experimental results show voltage degradation as a function of current density as can be expected. However, the slopes of the lines in Fig. 3 do not precisely correlate. This could be due to the stack resistance. In the model this term is taken as a constant value rather than a function of current. In reality stack resistance would likely be dependent on current density. There are two phenomena which could explain the stack resistance; non-uniform temperature and current reversal. In the case of the model a uniform stack temperature is assumed. In practice temperature would vary within the stack creating cells or areas within a cell with lower voltage. There would also be areas in which the temperature and voltage were increased; however, the overall effect would be a reduced voltage due to the non-linear relationship between temperature and voltage. The second possible cause of the stack resistance is the occurrence of current reversal due to the system design. The prototype SOFC system is comprised of 2 Siemens Technologies Beta units. Each Beta unit consists of 24 cells with 8 in series and 3 in parallel. If any of the 3 sets of 8 cells in series are producing different voltages then it is possible for current backflow and an associated voltage loss. Modelling of this issue is challenging because temperature, species and flow information would have to be known throughout the entire stack in order to individually calculate each cells voltage and current production. As a result the stack resistance is left as a constant parameter.

Fig. 4 presents a comparison of the model results for η_{FCPM} and the net electrical power (P_{el}). As in Fig. 3, the data used only for validation and not for calibration is termed "Validation". The model and experimental results show good correlation; the average relative and root mean square errors for η_{FCPM} were 1.3 and 0.53%, respectively. The figure demonstrates the role that the BOP components as well as the auxiliary burner fuel flow have on η_{FCPM}. Although with increasing power, η_{FCPM} initially drops until 3300 W, it begins to increase again after that. This might seem counter intuitive if one considers only that voltage losses increase with P_{el} and directly affect η_{FCPM} (Fig. 3). However, as P_{el} is increased the cell is able to maintain hotter temperatures and the burner is needed less frequently resulting in higher η_{FCPM}. Furthermore, the higher temperatures result in higher reaction rate kinetics within the cell which also improves η_{FCPM}.

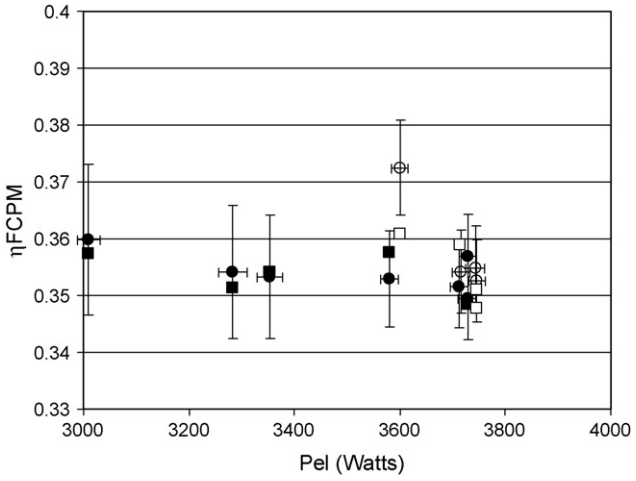

Fig. 4. Comparison of model and experimental results for stack η_{FCPM} as a function of P_{el}; experimental data used to calibrate model (●), model predictions corresponding to calibration experiment (■), experimental data used to validate model (○), model predictions corresponding to validation experiments (□).

4. Parametric study

One advantage to system-level models such as the Annex 42 is that they allow for the evaluation of different operating parameters with respect to their interaction between coherent device and the environment in which it will be installed. Namely the effects of altering parameters such as U_f, temperature and excess air ratio can be evaluated against the FCPM performance on a whole rather then just cell voltage as would be the case with a cell level model.

4.1. Impact of fuel utilization on system performance

Fig. 5a and b present the results of the U_f analyses, the figure demonstrates the dependence of cell voltage on U_f: as U_f increase the voltage decreases. This result is logical considering that a lower U_f results in higher partial pressure or concentration of the reactants at the anode electrolyte interface available for the electrochemical reactions. The relationship is linear after a U_f of 0.67. In the analyses the average temperature of the FCV was 1245 K (Calibration data 1, Table 1); however, at U_f below 0.67 the un-reacted fuel combusts and cause the temperature to rise (Fig. 5b). The increased temperature improves the voltage performance of the fuel cell.

From Fig. 5a it can be seen that U_f does not have as large an effect on η_{FCPM} as it does on voltage. The effect is also not as straightforward. Between U_f of 0.64 to 0.72, η_{FCPM} increases. This may be counter intuitive as the stack voltage is decreasing. However, the reduced voltage results in more heat generation in the cell raising its temperature. The raised temperature means less fuel needs to be combusted in the stack burner to maintain the set point temperature. At a U_f of 0.78, η_{FCPM} begins to decrease. This is because U_f is so high that there is not enough unreached fuel available for later combustion to maintain the operating temperature in the cell. As a result more fuel is required by the stack burner and η_{FCPM} would drop. Overall the effect of U_f on η_{FCPM} is not substantial in the range presented in Fig. 5a. The nominal U_f of the prototype system was 0.73–0.76 during the experiments.

4.2. Set point temperature

Fig. 6 presents the results from the temperature analyses and its effects on system performance. During this analysis U_f was held constant at 0.76 and the average P_{el} was 3010 W. An upper and lower (burner off and on) were set for each simulation run 5 K apart:

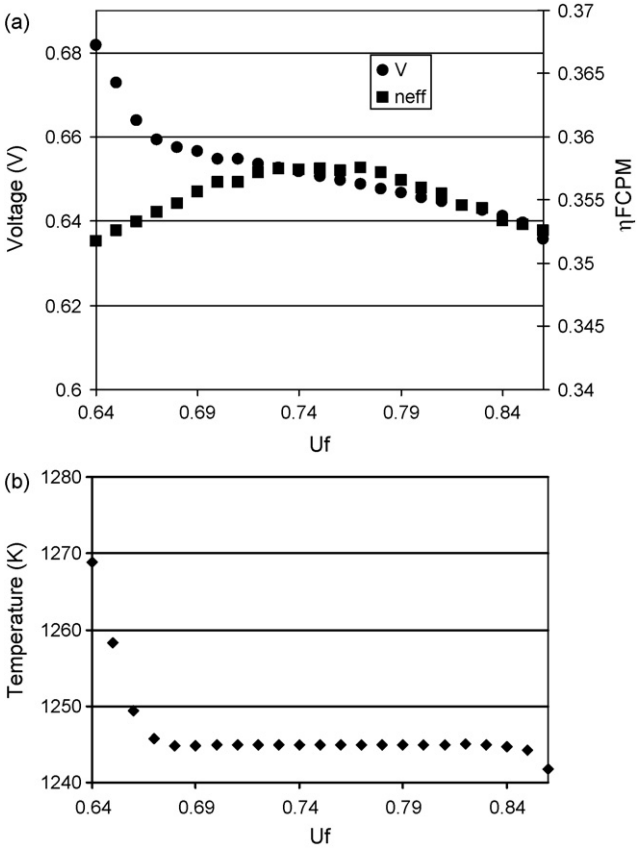

Fig. 5. Simulation results showing the effect of U_f on (a) voltage and η_{FCPM} (b) average stack temperature. All other parameters held constant, including excess air ratio and set point temperature.

the average temperature is presented in Fig. 6. Fig. 6 demonstrates the strong correlation between temperature and voltage performance of the cell. The relationship is polynomial (quadratic) with voltage increasing with temperature. The effect is expected due to the high temperature dependences of the polarization losses, especially ohmic.

Similarly to the U_f results, the effect of temperature on the entire system is not as straightforward as the effect on voltage. At temperatures bellow 1220 K, η_{FCPM} drops off due to increased voltage losses. At temperatures above 1260 K, the amount of fuel

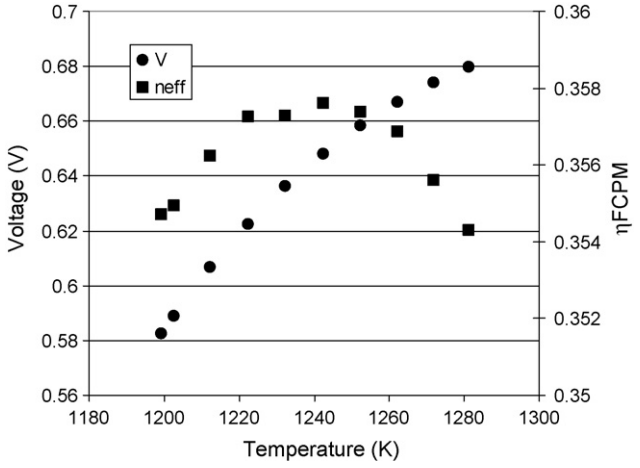

Fig. 6. Effect of average stack temperature on voltage and η_{FCPM}. All other parameters held constant, including excess air ratio and U_f.

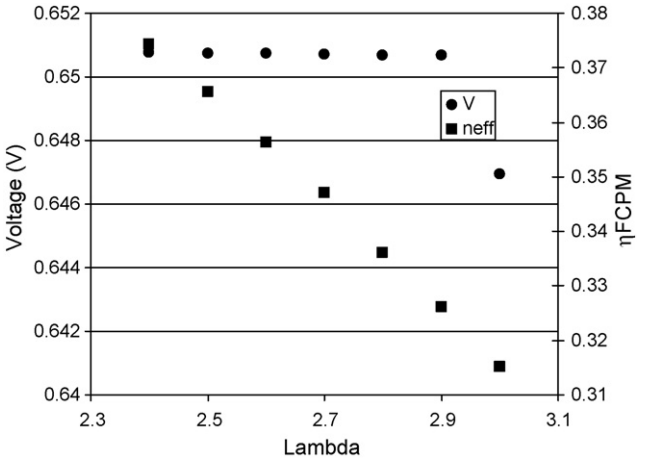

Fig. 7. Effect of excess air ratio (lambda) on voltage and η_{FCPM}. All other parameters held constant, including and set point temperature and U_f.

required by the stack burner outweighs the improved voltage performance associated with increasing temperature, and η_{FCPM} drops off. Between temperatures of 1220–1260 K, η_{FCPM} is steady. In that range the voltage is increasing as is the amount of fuel required by the stack burner. Based on the simulation results, the effect of improved voltage performance and increased stack burner fuel consumption balance out causing η_{FCPM} to remain steady. In practice this region of steady η_{FCPM} is likely smaller. Although uniform stack temperature is assumed, non-uniform temperature distribution in the stack could occur. As mentioned in Section 3, if this occurs, cells or areas within a cell would experience lower then average temperatures. The "power" relationship between voltage and temperature would magnify those areas of reduced temperature resulting in decreased η_{FCPM} compared to those values reported by the model.

4.3. Excess air ratio

Finally, Fig. 7 presents the effects of excess air ratio on η_{FCPM} and cell voltage. As excess air ratio is increased, η_{FCPM} decreases. This result is logical from a thermodynamic perspective. The additional air added to the system must be heated, which requires more energy and reduces the η_{FCPM}. There is no noticeable effect on cell voltage until the excess air ratio exceeds 2.9, after which voltage drops off sharply. This drop off is likely due to the model no longer being able to maintain the setpoint temperature. Logically then, reducing excess air ratio as much as possible (down to stoichiometry) would appear to be ideal. In practice, there are two reasons why this cannot be done. First, if excess air is reduced too much then insufficient oxygen will be available at the reaction sites, and due to the mass transport limitations, a substantial voltage loss could occur. Second, excess air ratio provides additional cooling capacity to the system if temperatures rise.

5. Conclusions

A semi-mechanistic fuel cell power module model has been developed for a SOFC and implemented into the ESP-r building simulation program to enhance the Annex 42 SOFC cogeneration model. Based on the results (Figs. 3 and 4) the new model demonstrated good correlation with experimental data. Data produced by the model was within the uncertainty of the measurements and produced a slope of 0.45 mV A^{-1} compared to 0.44 for the measured data.

The general approach for stack and system-level models found in the current literature consisted of a cell level model multiplied by the number of cells in the stack, coupled with an energy balance of the stack or system. The current research found that additional voltage losses occur at the stack level compared to the cell level. Literature reviewed for the current research did not determine this because model results were compared to single cell data rather then stack data. The stack resistance term was added to the model to account for these losses. Although the term was not large (3.55 mV per cell), it still demonstrated that consideration must be given when applying a cell model to a stack or system.

Both the model predictions and experimental data showed that between a P_{el} of 3000 and 3700 (W) the average stack temperature can rise from less then 1245 K to greater then 1260 K. These high temperatures and sensitivity to operational changes show that thermal management is important in SOFCs. The excess air ratio and the stack burner can be used to partially control temperature; however, the degree of control is limited. These are important considerations in the design and operation of SOFC cogeneration systems.

The current research demonstrated that improved cell voltage results in less heat generation (voltage losses or irreversibilities result in heat generation in SOFCs). If the reduced heat generation results in a temperature reduction sufficient to activate the stack burner then little or no gain in efficiency of the entire system will occur. Therefore, as improvements are made to the cell, better thermal management and materials with better tailored properties must also be investigated to offset the reduced heat generation due to irreversibilities.

Acknowledgments

The authors are grateful to the Department of Natural Resources Canada (NRCan) for financial support as well as provision of experimental data. The work was also supported by the Natural Sciences and Engineering Research Council of Canada (NSERC).

References

[1] S.C. Singhal, K. Kendall, High-temperature Solid Oxide Fuel Cells: Fundamentals, Design, and Application, 1st ed., Elsevier Advanced Technology, New York, 2003.
[2] S.H. Chan, H.K. Ho, Y. Tian, J. Power Sources 109 (2002) 111–120.
[3] S.H. Chan, H.K. Ho, Y. Tian, Int. J. Hydrogen Energy 28 (2003) 889–900.
[4] R.J. Braun, S.A. Klein, D.T. Reindl, J. Power Sources 158 (2006) 1290–1305.
[5] P. Lisbona, A. Corradetti, R. Bove, P. Lunghi, Electrochim. Acta 53 (2007) 1920–1930.
[6] A.D. Hawkes, P. Aguiar, B. Croxford, M.A. Leach, C.S. Adjiman, N.P. Brandon, J. Power Sources 164 (2007) 260–271.
[7] OPA, Ontario's Integrated Power System Plan, Ontario Power Authority, Toronto, 2007.
[8] I. Beausoleil-Morrison, A. Schatz, F. Marĭechal, HVAC&R Res. 12 (3A) (2006) 641–667.
[9] N. Kelly, I. Beausoleil-Morrison, Specifications for modeling Modelling Fuel Cell and Combustion-Based Residential Cogeneration Device within Whole-Building Simulation Programs, IEA/ECBS's Annex 42 Report, 2007, ISBN 978-0-662r-r47116-5.
[10] I. Beausoleil-Morrison (Ed.), An Experimental and Simulation-based Investigation of the Performance of Small-scale Fuel Cell and Combustion-Based Cogeneration Devices Serving Residential Buildings, International Energy Agency/Energy Conservation in Buildings and Community Systems Programme Annex 42 Report, 2008.
[11] J.A. Clarke, Energy Simulation in Building Design, Oxford, 2001.
[12] D. Sanchez, R. Chacartegui, A. Munoz, T. Sanchez, Int. J. Hydrogen Energy 33 (2008) 1834–1844.
[13] S. Nagata, A. Momma, T. Kata, K. Yasuhiro, J. Power Sources 101 (2001) 60–71.
[14] U.G. Bossel, Final Report on SOFC data facts and figures, Swiss Federal Office of Energy, Berne, CH, 1992.
[15] K.J. Yoon, P. Zink, S. Gopalan, U.B. Pal, J. Power Sources 172 (2007) 39–49.
[16] S. Campanari, P. Iora, J. Power Sources 132 (2004) 113–126.
[17] A.V. Akkaya, Int. J. Energy Res. 31 (2007) 79–98.
[18] S. Krumdieck, S. Page, S. Round, J. Power Sources 125 (2004) 189–198.
[19] J. Padulles, G.W. Ault, J.R. McDonald, J. Power Sources 86 (2000) 495–500.
[20] S.H. Chan, K.A. Khor, Z.T. Xia, J. Power Sources 93 (2001) 130–140.

[21] K. Nisancioglu, Proceedings of the IEA Workshop on Mathematical Modelling, Charmey, 1989, pp. 87–98.
[22] J.W. Kim, A.V. Virkar, K.Z. Fung, K. Mehta, C. Singhal, J. Electrochem. Soc. 146 (1999) 69–78.
[23] B. Todd, J.B. Young, J. Power Sources 110 (2002) 186–200.
[24] W. Zhang, E. Croiset, P.L. Douglas, M.W. Fowler, E. Entchev, Energy Convers. Manage. 46 (2005) 181–196.
[25] K Tanaka, C. Wen, K. Yamada, Fuel 79 (2000) 1493–1507.
[26] X.J. Wu, X.J. Zhu, G.Y. Cao, H.Y. Tu, Simul. Model. Pract. Theory 16 (2008) 399–409.
[27] P.G. Bavarsad, Int. J. Hydrogen Energy 32 (2007) 4591–4599.
[28] I. Beausoleil-Morrison, The empirical validation of a model for simulating the thermal and electrical performance of fuel-cell micro-cogeneration devices, J. Power Sources 195 (5) (2010) 1416–1426.

Glossary

A: constant for equilibrium constant calculation (K^{-4})
A_{cell}: area perpendicular to current-flow (cm^2)
A_{int}: area perpendicular to current-flow for the interconnect (cm^2)
B: constant for equilibrium constant calculation (K^{-3})
C: constant for equilibrium constant calculation (K^{-2})
CH_4: chemical formula methane
C_nH_m: chemical formula generic hydrocarbon
CO: chemical formula carbon monoxide
CO_2: chemical formula carbon dioxide
D: constant for equilibrium constant calculation (K^{-1})
D_{eff}: effective diffusion coefficient ($cm^2\ s^{-1}$)
$D_{H_2\text{-}H_2O}$: binary diffusion coefficient ($cm^2\ s^{-1}$)
$D_{i,k}$: Knudsen diffusion coefficient ($cm^2\ s^{-1}$)
E: constant for equilibrium constant calculation
E_{act}: activation energy (kJ)
E_r: Nernst potential voltage (V)
F: Faradays constant (coulombs mol^{-1})
H: enthalpy flow ($J\,kmol^{-1}\ s^{-1}$)
H_2O: chemical formula water
H_2: chemical formula hydrogen
i: current density ($A\,cm^{-2}$)
I_{cell}: cell current (A)
i_L: limiting current density ($A\,cm^{-2}$)
i_o: exchange current density ($A\,cm^{-2}$)
K_s: equilibrium constant gas-shift reaction
L: thickness (cm)
L_{cell}: cell length (z-dir)
LHV_{fuel}: lower heating value of the fuel ($J\,kmol^{-1}$)
m: empirical coefficient (exchange current density equation)
M: molar mass ($kg\,mol^{-1}$)
MC_ρ: thermal capacitance ($J\,K^{-1}$)
$n_{cells\text{-}parallel}$: number of cells in parallel
$n_{cells\text{-}series}$: number of cells in series
n_e: electrons per molecule of fuel
$N_{fuel\text{-}stack}$: fuel flow rate to the stack ($kmol\,s^{-1}$)
$N_{fuel\text{-}burn}$: fuel flow rate to the stack burner ($kmol\,s^{-1}$)
O_2: chemical formula oxygen
p: partial pressure
P: pressure (bar)
$Path_{el}$: radial distance (circumference) of the electrolyte (cm)
P_{cell}: cell pressure (bar)
$P_{dc,ann}$: FCPM parasitic power draw (W)
$P_{dc,comp}$: power draw of the BOP components (W)
P_{IV}: power loss due to voltage drop between stack and PCU (W)
P_{el}: electrical power required by power conditioning unit (W)
P_{stack}: electrical power produced by the fuel cell stack (W)
$q_{skinlosses}$: heat losses (W)
R: universal gas constant ($bar\,m^3\,K^{-1}\,mol^{-1}$)
r_{CH_4}: reformation rate methane ($mol\,s^{-1}$)
R_{eq}: area specific equivalent ohmic resistance ($\Omega\,cm^2$)
R_{ohm}: area specific ohmic resistance ($\Omega\,cm^2$)
r_{por}: pore length (cm)
T: temperature (K)
t: time (s)
$T_{air,in\text{-}FCPM}$: temperature of the air entering the FCPM (K)
$T_{air,in\text{-}FCV}$: temperature of the air entering the FCV (K)
T_{FCV}: temperature of the FCV (K)
$T_{fuel,in\text{-}FCPM}$: temperature of the fuel entering the FCPM (K)
$T_{fuel,in\text{-}FCV}$: temperature of the fuel entering the FCV (K)
$T_{product\text{-}FCPM}$: temperature of the product gases leaving the FCPM (K)
U_f: fuel utilization rate
V_{act}: activation polarization (V)
V_{cell}: fuel cell voltage (V)
V_{conc}: concentration polarization (V)
V_{ohm}: ohmic losses (V)
V_{SR}: stack resistance voltage (V)
x: Molar flow rate methane ($kmol\,s^{-1}$)
y: Molar flow rate carbon monoxide ($kmol\,s^{-1}$)
z: Molar flow rate hydrogen ($kmol\,s^{-1}$)

Greek letters

β: charge transfer coefficient
β_i: heat transfer coefficient
γ: pre-exponential factor
δ: ratio of Knudsen to total diffusion
ε: porosity
$\varepsilon_{ann\text{-}0}$: calibration coefficient for BOP power draw (W)
$\varepsilon_{ann\text{-}1}$: calibration coefficient for BOP power draw (W^{-1})
$\varepsilon_{IV\text{-}0}$: calibration coefficient for BOP power draw (W)
$\varepsilon_{IV\text{-}1}$: calibration coefficient for BOP power draw (W^{-1})
η_{FCPM}: efficiency of the fuel cell power module
η_{FCS}: efficiency of the fuel cell stack
ν: diffusion volume (cm^3)
τ: tortuosity
σ: conductivity ($\Omega^{-1}\,cm^{-1}$)

Superscripts

an: anode
ca: cathode
I: inlet condition
i: placeholder for species (i.e. H_2, CH_4, etc.)

Subscripts

A–B: molecules participating in binary diffusion
air: air entering the system
an: anode
ca: cathode
el: electrolyte
fuel: fuel entering the system
I: inlet condition
i: placeholder for species (i.e. H_2, CH_4, etc.)
int: interconnect
products: product gases leaving the system
stack-burn: referring to the stack burner